Chlorophyll *a* Self-assembly in Polar Solvent–Water Mixtures†

Radka Vladkova*

Institute of Biophysics, Bulgarian Academy of Sciences, Sofia, Bulgaria

ABSTRACT

The conversion of chlorophyll *a* (Chl *a*) monomers into large aggregates in six polar solvents upon addition of water has been studied by means of absorption, fluorescence spectroscopy and fluorescence lifetime measurements for the purpose of elucidating the various environmental factors promoting Chl *a* self-assembly and determining the type of its organization. Two empirical solvent parameter scales were used for quantitative characterization of the different solvation properties of the solvents and their mixtures with water. The mole fractions of water $f_{1/2}$ giving rise to the midpoint values of the relative fluorescence quantum yield were determined for each solvent, and then various solvent–water mixture parameters for the $f_{1/2}$ values were compared. On the basis of their comparison, it is concluded that the hydrogen-bonding ability and the dipole–dipole interactions (function of the dielectric constant) of the solvent–water mixtures are those that promote Chl *a* self-assembly. The influence of the different nature of the nonaqueous solvents on the Chl aggregation is manifested by both the different water contents required to induce Chl monomer → aggregate transition and the formation of two types of aggregates at the completion of the transition: species absorbing at 740–760 nm (in methanol, ethanol, acetonitrile, acetone) and at 667–670 nm (in pyridine and tetrahydrofuran). It is concluded that the type of Chl organization depends on the coordination ability and the polarizability (function of the index of refraction) of the organic solvent. The ordering of the solvents with respect to the $f_{1/2}$ values—methanol < ethanol < acetonitrile < acetone < pyridine < tetrahydrofuran—yielded a typical lyotropic (Hofmeister) series. On the basis of this solvent ordering and the disparate effects of the two groups of solvents on the Chl *a* aggregate organization, it is pointed out that the mechanism of Chl *a* self-assembly in aqueous media can be considered a manifestation of the Hofmeister effect, as displayed in the lipid-phase behavior (Koynova *et al., Eur. J. Biophys.* **25, 261–274, 1997). It relates to the solvent ability to modify the bulk structure and to distribute unevenly between the Chl–water interface and bulk liquid.**

INTRODUCTION

The process of photosynthesis in various organisms (plants, algae, photosynthetic bacteria) starts with the high efficient light collection by so-called antenna complexes. Chlorophyll *a* (Chl *a*)‡ and bacteriochlorophyll *c* (Bchl *c*) are the major antenna pigments in higher plants and in green photosynthetic bacteria, respectively. Their organization as high efficient light collectors is of crucial importance for the functioning of the overall photosynthetic unit. In contrast to green photosynthetic bacteria, where strong pigment–pigment interactions determine the organization of chlorosomal Bchl *c* and *d* (1), in higher plants the polypeptide amino acid residues bind and organize the antenna Chl *a* and *b* by specific and nonspecific interactions (2). Despite the fact that the structure of several Chl–protein complexes is known at near atomic resolution, the molecular mechanism for their assembly and structural stability remains unclear.

One of the reasons is that the mechanism for Chl self-assembly in aqueous media is also unclear. That such knowledge is of importance is evident by the same effects that medium composition has on both the chlorosomes (3) and Bchl *c* and *d* aggregates in aqueous media (4) or on chloroplast fragments (5) and Chl *a* aggregates in aqueous solvents (6). While the formation of Chl aggregates in various organic solvent–water mixtures is well documented (6–18), little is known about the contribution of the structure and properties of the medium for the assembly and stabilization of different Chl aggregate organizations in aqueous media. A study on the relationship between the Chl aggregation and solvent structure and properties can lead to an elucidation of the mechanism for Chl assembly and dissolution in aqueous media and consequently in the photosynthetic antenna complexes.

Despite the well-documented formation of Chl *a* aggregates in organic solvent–water mixtures, there are only a few studies aimed at clarifying and quantifying the dependence of the process of Chl *a* aggregation on the properties of the medium. In earlier studies, only the physical (nonspecific)

---

*To whom correspondence should be addressed at: Institute of Biophysics, Bulgarian Academy of Sciences, Acad. G. Bonchev St., Bl. 21, 1113 Sofia, Bulgaria. Fax: +359-2-9712493; e-mail: vladkova@obzor.bio21.bas.bg

‡*Abbreviations:* ACE, acetone: ACN, acetonitrile; Bchl, bacteriochlorophyll; Chl, chlorophyll; DMSO, dimethylsulfoxide; EtOH, ethanol; FWHM, full width at half maximum; MeOH, methanol; PYR, pyridine; RR, resonance Raman; THF, tetrahydrofuran.

parameters of the medium, the dielectric constant ε (19) and the molecular refraction and molecular polarization of the solvent–water mixtures (6) had been considered. Later studies focused mainly on the detailed description of the spectral properties of the different dimers and aggregates formed in particular polar solvent–water mixtures (15–18). The different spectral forms are ascribed to the bulk properties of the medium (15,18) or to the specific Chl–solvent interactions characteristic of some particular solvents (16,17). Uehara *et al.* (16,17) found a correlation between solvent structure and selectively formed Chl *a* aggregates absorbing at 683–695 nm. Recently, Oba *et al.* (20) presented the solvent composition dependence of Chl *a'* aggregation in aqueous methanol as a phase diagram. They concluded that the Chl *a'* aggregation is similar to a phase separation (a micellization) of nonionic surfactant in water, based on the similarity in critical behavior. However, if the different specific and nonspecific solvation properties of the aqueous medium are not taken into account, and most importantly are not quantitatively described, it is difficult to evaluate the main principles governing the process of Chl association in various aqueous media.

In view of the difficulties applying theoretical expressions for calculating all interactions in three-component systems, another route to establishing the role of the medium is to use some of the empirical solvent scales as quantitative measures of both specific and nonspecific solvating properties. There are a number of empirical parameters that take into account all solute–solvent interactions at a microscopic level (21,22). Moreover, several empirical parameters have already been successfully applied in model studies on Chl *a* and Bchl *a* (23–25). The parametrization of various aqueous media should simplify evaluation of the common solvent effect on Chl aggregation in different systems.

To our knowledge, the present work is the first attempt to use empirical solvent parameters for quantitative description of the different specific and nonspecific solvation properties of the medium during the process of Chl *a* self-assembly in six polar solvent–water mixtures. Based on this, it was possible to correlate the process of Chl aggregation as well as the type of aggregates formed at the completion of transition with the solvent parameters. The established correlation allowed us to consider the polar solvent effect on Chl *a* aggregation in aqueous media as a manifestation of the Hofmeister effect, just as it is displayed concerning the structural stability of two other biomolecular assemblies: proteins and lipids. Based on the proposed mechanism, the solvent effect studied here is directly connected to the spectra–structure–function relationship *in vivo*.

MATERIALS AND METHODS

Materials. Chlorophyll *a* was purchased from Sigma Chemical Co. (catalogue no. C-6144) and used without further purification. All solvents used were freshly dried and distilled prior to use. Methanol (MeOH) and ethanol (EtOH) (p.a.) were allowed to stand over CaO, then dried by Mg turnings; acetone (ACE), acetonitrile (ACN) and carbon tetrachloride (CCl$_4$) (Fluka) were allowed to stand over CaCl$_2$, and pyridine (PYR) and tetrahydrofuran (THF) (Merck) over solid NaOH and KOH, respectively. After that, the solvents were filtered, distilled and stored over activated 4 Å molecular sieves (Merck). Water was doubly distilled.

Sample preparations. The stock solution of 1 mg Chl *a* in 10 mL CCl$_4$ was prepared and kept in the dark at −20°C. For every series of solvent–water mixtures, equal amounts of the stock solution were put into test tubes and CCl$_4$ was evaporated with a stream of dry nitrogen. The thin films of Chl *a* were dissolved in the desired amount (vol%) of the solvent of interest, and then the required amount of water was added. The closed test tube containing the solution was then shaken by hand several times. The concentration of Chl *a* was determined by its optical density (absorbance) in the red band peak using the molar extinction coefficient in each single solvent (26). The maxima of the absorption bands and their relative intensities were in good agreement with the published values for these solvents. For every series of solvent–water mixture the concentration of Chl was the same, usually in the range of 2.7–2.9 × 10^{-6} *M*. The studied concentration range was 2.7–5.7 × 10^{-6} *M*.

Absorption and fluorescence measurements. Absorption measurements were performed on a Specord UV/visible double-beam spectrophotometer (Carl Zeiss, Germany). The spectra are presented as absorption, 1 − T (T = transmission), in order to better see the details of the spectral transformations. Identical results are observed for a concentration of 2.7 or 5.7 × 10^{-6} *M*.

The fluorescence spectra were recorded on a Perkin-Elmer MPF 44B spectrofluorometer at right angle with respect to the excitation. The excitation wavelength was 430 nm; the spectral bandwidths were 4 nm. The relative fluorescence quantum yields ϕ^w/ϕ^o of Chl *a* in solvent–water mixtures *versus* that in the pure organic solvent were determined by dividing the ratio of the integrated fluorescence intensities (600–770 nm spectral range) of both samples by the ratio of their absorption, (1 − T), at the excitation wavelength. The experimental error in the quantum yield was estimated to be 10%. Fluorescence lifetime measurements were done using a laser pulse fluorometer LIF 200 (ZWG, Berlin; excitation source: nitrogen laser [λ_{exc} = 337.1 nm, pulse duration ≈500 ps]; detection system: photodiodes with boxcar integrator, instead of monochromator-only cutoff filters could be utilized). The apparatus is described in detail in Dähne *et al.* (27). Laser pulse intensity was around 1 × 10^{14} photons/cm^2. The fluorescence lifetimes were determined by using the standard deconvolution procedure.

Each sample was measured 1 min after preparation at appropriate time intervals until temporal evolution in the spectra was accomplished. Measurements were carried out in closed 1 cm quartz cuvettes at 25°C, because data on the used solvent and solvent–water mixture parameters are available in the literature at this temperature.

Parameters of the solvents and solvent–water mixtures. The refractive index (n) measurements of the solvents and solvent–water mixtures were made at 25°C with an Abbe-type refractometer from Carl Zeiss Jena.

The interpolated values of the dielectric constant ε for different solvent–water mixtures were taken from the available literature data (see references in Table 1) with the exception of ACN–water mixtures. They were calculated using Eq. 22 in Hasted (31).

The values of the solvent polarity parameter E$_T$(30) for the mixtures were taken from the literature (see references in Table 1), except for the ACN– and THF–water mixtures. Knowing that the E$_T$(30) values of ACN were intermediate between those of EtOH and ACE (22), the intermediate value between the EtOH– and ACE–water mixtures (33) at the respective vol% water was taken for the ACN–water mixture. The same was done for THF–water using the established similarity between THF and dioxane (34); we took the values of E$_T$(30) for the latter solvent in mixture with water that is known (33).

The parameters electrophilicity (E) and nucleophilicity (B) of the solvent–water mixtures were calculated as additive functions of their mole fractions, according to Palm (32).

RESULTS AND DISCUSSION

Chl *a* monomer → aggregate transition

For the purpose of the present work, six polar solvents were selected that are of very different chemical nature and cover a wide range of values of medium physical parameters such as index of refraction and dielectric constant (Table 1). As is shown in Table 1 these solvents give rise to four types of

Table 1. Characterization of Chl *a* solutions: type of specific solvation of Chl *a,* index of refraction (*n*) and dielectric constant (ϵ), Dimroth and Reichardt's solvent polarity parameter $E_T(30)$ (in kcal/mol) and Koppel and Palm's empirical solvent parameters: polarity (*Y*), polarizability (*P*), electrophilicity (*E*) and nucleophilicity (*B*)

Solvent*	Type of solvate†	n‡	ϵ§	$E_T(30)$‖	Y	P	E¶	B¶
Water		1.3330	78.48	63.1	0.9627	0.2057	21.8	156
MeOH	L_2H	1.3285	32.66	55.5	0.9134	0.2032	14.9	218
EtOH	L_1H	1.3614	24.3	51.9	0.8859	0.2215	11.6	235
ACN	L_1	1.3440	36.0	46.0	0.9211	0.2118	5.2	160
ACE	L_1	1.3589	19.1	42.2	0.8578	0.2201	2.1	224
PYR	L_2	1.5101	13.06	40.2	0.8008	0.2991	0	472
THF	L_2	1.4076	7.39	37.4	0.6805	0.2465	0	287

*Arranged by decreasing $E_T(30)$ values (fourth column).
†L_i denotes the coordination number (=i + 4) of the Mg atom; L_iH denotes additional hydrogen bonds with the keto carbonyl group of Chl *a* (23,24,28,29).
‡Measured at 25°C.
§Values at 25°C taken from Landolt-Börnstein (1959) Vol. II/6, pp. 750–753, Springer-Verlag, Berlin for water, MeOH, ACE and THF; for EtOH from Åkerlöf (30); for ACN from Gutman (21), p. 148, and for PYR from Hasted (31), p. 424.
‖At 25°C from Reichardt (22), pp. 270–271.
¶From Palm (32), pp. 333–334.

specific solvates of monomeric Chl *a* that also imitate different *in vivo* pigment environments. The parameters used for the quantitative characterization of different specific and nonspecific solvation properties of the solvents and water are also listed in Table 1. In order to assess the role of the different properties of the medium on Chl association only, the concentration of Chl *a* was low and kept constant in all solvents and solvent–water mixtures. By varying the molar ratio of solvents and water that are miscible in all proportions, it was possible to change all medium parameters and thus to induce the association of Chl molecules. Figure 1 shows the effect of the increase of water content on the relative fluorescence quantum yield ϕ^w/ϕ^o (normalized with respect to those of monomeric Chl *a* in the respective non-aqueous solvent). These curves were used as a diagnostic tool for the degree of Chl monomer → aggregate transition.
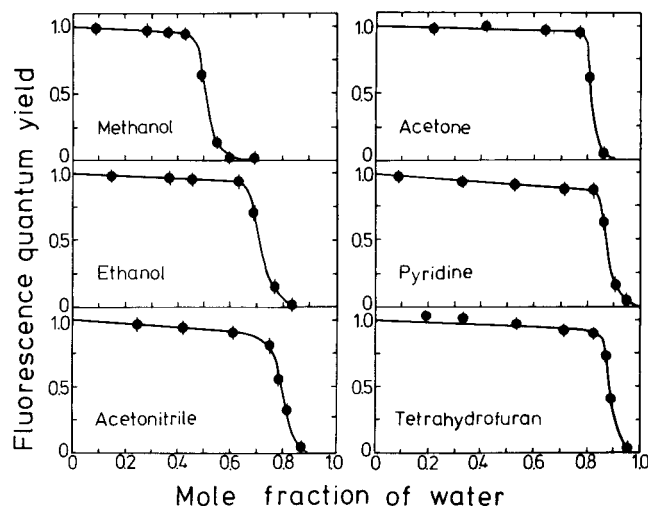

Figure 1. Normalized fluorescence quantum yield of Chl *a* (relative to the respective nonaqueous solvent) in different solvent–water mixtures as a function of the mole fractions of water. The concentration of Chl *a* was kept low and constant ($2.7–2.9 \times 10^{-6}$ *M*), while the solvent/water ratio was varied.

The grounds to use ϕ^w/ϕ^o as a measure of the fraction of the monomeric Chl molecules in the mixtures were (1) by definition it directly yields the number of fluorescing molecules; (2) these fluorescing molecules are the monomeric Chl *a* because the excitation is at 430 nm, *i.e.* not at the wavelength longer than the Soret absorption maximum, a region for excitation of aggregated Chl *a* (20); (3) it is well known that aggregated forms of Chl *a* in dilute polar solvent–water mixtures are practically nonfluorescent or nearly so at room temperature (9,12) and the possible part of their fluorescence ($\leq$1% with respect to the monomeric ones) is included in the error limits connected with the calculation of the relative quantum yields (relative error at the highest mole fractions of water $\pm$10–15%).

Figure 1 demonstrates that the effect of water on the relative quantum yield of Chl *a* can be divided into three zones. In zone I, the linearly approximated part of the curves, the changes in ϕ^w/ϕ^o are small and continuous depending on the pure solvent. These changes are ascribed to changes in the dielectric constant of the solutions of the monomeric Chl *a* (13) and also to changes in the type of specific solvation of monomeric Chl *a* (14,35) (see below). In zone II, termed here the transition zone, there is an abrupt decrease of fluorescence quantum yield, *i.e.* a strong decrease in the number of monomeric Chl *a* with an increase in water content. The mole fractions of water at which the quenching of Chl *a* fluorescence starts, *i.e.* the onset of the monomer → aggregate transition, in each of the solvent–water mixtures are different and increase in succession MeOH < EtOH < ACN < ACE < PYR < THF. This result indicates that the different solvents exert different association power on Chl *a* in mixtures with water and will be discussed later. In zone III, there is no fluorescence, *i.e.* the transition is already completed, and all the monomeric Chl exists in aggregate form. In this study, the effect of solvent–water composition on the aggregation of Chl *a* is examined until the full quenching of the monomeric Chl fluorescence is accomplished. As a whole, the values of the mole fractions of water, marking the transition zone, are in accordance with previous studies (6,12,13,15).

Table 2. Mole fractions of water $f_{1/2}$ in different solvent–water mixtures corresponding to the midpoint value of the relative fluorescence quantum yield curves of Chl *a,* established from Fig. 1

Solvent*	$f_{1/2}$ (±0.01)	Concentration of water† (vol/vol) %	$n_{1/2}$‡	$\epsilon_{1/2}$§
MeOH	0.51	31.6 ± 0.9	1.3423 ± 0.0002	50.4 ± 0.4
EtOH	0.72	44.3 ± 1.2	1.3608 ± 0.0002	50.5 ± 0.5
ACN	0.79	56.3 ± 1.5	1.3462 ± 0.0003	60.1 ± 0.6
ACE	0.82	52.8 ± 1.7	1.3583 ± 0.0006	53.7 ± 1.2
PYR	0.87	59.9 ± 2.2	1.4088 ± 0.0040	55.5 ± 1.0
THF	0.88	61.9 ± 2.3	1.3684 ± 0.0020	52.2 ± 1.8

*See footnote *, Table 1.
†Calculated from $f_{1/2}$ ± SD.
‡Measured at 25°C.
§See footnote § in Table 1, except for ACN. Its value was calculated using Eq. 22 in Hasted (31), p. 412.

In order to assess which properties of the medium promote Chl association, the midpoints of the fluorescence quenching curves with respect to the mole fractions of water were estimated. At that point, the fraction of monomeric Chl *a* is the same for all mixtures, irrespective of the cooperativity of the transition (7) and the intermediate small aggregates (dimers, trimers, *etc.*) formed during the transition. The idea was to find a characteristic parameter of the medium that has similar values in all different solvent–water mixtures at the midpoint of the transition. In this way we intended to decipher the interactions responsible for Chl *a* self-assembly.

Table 2 summarizes the mole fraction of water $f_{1/2}$ values for all mixtures that correspond to the midpoint of each ϕ^w/ϕ^o curve, presented in Fig. 1. The values of $f_{1/2}$ in the different mixtures increase in the same order as at the onset of the transition.

The quantitative characterization of the different medium properties for the $f_{1/2}$ mixtures is done by the values of their physical constants (Table 2) and empirical parameters (Table 3). The comparison of the relative deviations of the weighted mean values (36) for all parameters, as well as the sum of their relative deviations (Table 3) shows that these devia-

tions are smallest for the $E_T(30)$ parameter and for two of the four-parametric scale of Koppel and Palm, $Y_{1/2}$ and $E_{1/2}$. Taking into account that these deviations are within the same range as the maximum error limits imposed by the $f_{1/2}$ values (≤4%, Table 2), it is clear that the values of the $E_T(30)$ parameter, and those of the $Y_{1/2}$ and the $E_{1/2}$ parameters can be taken as equal within the experimental error for all six mixtures. Note also that the pure solvents have very different empirical parameters (Table 1). Thus, irrespective of the kind of polar solvent, the monomer → aggregate transition takes place at certain values of the solvent parameters $E_T(30)$, Y and E. This result is convincing evidence that the properties of the medium, characterized by these parameters, are of primary importance for Chl *a* association in aqueous media.

How the medium promotes Chl *a* self-assembly

The empirical parameter polarity $E_T(30)$ from the single parametric approach of Reichardt and Dimroth as described by Reichardt in (22) is essentially a scale reflecting dipole–dipole interactions (expressed by the function of the dielectric constant, ϵ) with the addition of the hydrogen-bonding ability of the solvent (37). The $E_T(30)$ polarity scale is one of the various empirical scales introduced to characterize the solvation ability of solvents. In view of the complexity of solute–solvent interactions, it is beneficial to correlate the association of Chl *a* molecules in aqueous solutions with a single parameter.

The second quantitative approach used here gives the complete description of all specific and nonspecific solvating abilities of the solvents. It is noteworthy that the exact same two properties characterized by the $E_T(30)$ parameter are the properties characterized quantitatively by the parameters Y and E from the four-parametric approach of Koppel and Palm as described by Palm in (32). The nonspecific polarity parameter Y measures solvent polarization used in the form of the Kirkwood function $(\epsilon - 1)/(\epsilon + 2)$. Y characterizes the polarity of the solvent in terms of dipole moments. The larger the polarity of the medium, the larger the average dipole moment and the better the alignment of molecules.

Table 3. Empirical solvent parameters of the different solvent–water mixtures at $f_{1/2}$ mole fraction of water

Solvent	$E_T(30)_{1/2}$*	$Y_{1/2}$†	$P_{1/2}$†	$E_{1/2}$‡	$B_{1/2}$‡
MeOH	57.3 ± 0.1	0.9428 ± 0.0005	0.2109 ± 0.0001	18.4 ± 0.1	186.4 ± 0.6
EtOH	55.3 ± 0.1	0.9429 ± 0.0006	0.2211 ± 0.0002	18.9 ± 0.1	178.1 ± 0.8
ACN	56.1 ± 0.3	0.9517 ± 0.0005	0.2131 ± 0.0002	18.3 ± 0.2	156.8 ± 0.1
ACE	55.8 ± 0.3	0.9461 ± 0.0011	0.2198 ± 0.0004	18.3 ± 0.2	168.2 ± 0.7
PYR	54.7 ± 0.2	0.9478 ± 0.0009	0.2471 ± 0.0029	19.0 ± 0.2	197.1 ± 3.2
THF	55.8 ± 0.5	0.9447 ± 0.0019	0.2253 ± 0.0014	19.2 ± 0.2	171.7 ± 1.3
Weighted mean value§	56.1 ± 0.4	0.9463 ± 0.0014	0.2133 ± 0.0068	18.7 ± 0.2	158.2 ± 10.0
Relative SD‖ (%)	1.6	0.36	7.8	2.1	15.4
Sum of relative deviations¶ (%)	3.2	0.69	13.5	0.53	34.5

*Taken from Reichardt and Dimroth (33), except for ACN and THF (see Materials and Methods).
†Calculated using $n_{1/2}$ and $\epsilon_{1/2}$ values from Table 2.
‡Calculated as additive functions of $f_{1/2}$, according to Palm (32).
§Calculated according to Szabo and Rayner (36), ±SD.
‖Relative standard deviation of the weighted mean values.
¶Sum of the relative deviations of the range of each mixture value from the range of the weighted mean value.

This parameter reflects dipole–dipole (orientation) interactions. The specific solvation parameter electrophilicity (E) measures the Lewis acidity (electrophilic solvating power, hydrogen-bond donating ability).

Thus, the identical results obtained in this work by applying two quantitative approaches allow us to state that the association of Chl *a* depends on the hydrogen-bonding and orientation interactions of the aqueous media irrespective of the kind of polar solvent. It is important to note that until now these parameters have been used to characterize only the properties of the medium, *i.e.* the interactions within the bulk system. With respect to Chl *a,* these interactions can be considered indirect. Consequently, the conclusion is that the process of Chl *a* self-assembly in aqueous medium is a solvent-structure-induced process. The Chl molecules are forced to come together and to associate when the hydrogen-bonding and dipole–dipole interactions establish a certain degree of short- and long-range ordering in the bulk system qualitatively characterized by the values of parameters E and Y, respectively. The creation of a hydrogen-bond network in the system with or without the participation of the initial nonaqueous solvent in this network (38) is the driving force for Chl association in aqueous media. Thus, the correlation between the structure of the aqueous medium and Chl aggregation is established.

The solvents used arrange in the order MeOH < EtOH < ACN < ACE < PYR < THF with respect to the onset and $f_{1/2}$ values. The findings that the parameter polarizability (P) and nucleophilicity (B) are different at the midpoint of the transition indicates that these two parameters are a specific, peculiar feature for the particular solvents that determine their different power in mixtures with water to the self-assembly of Chl *a*. Considering the structure of the bulk system, this finding also means that these two parameters determine the graded solvent effect (MeOH < EtOH < ACN < ACE < PYR < THF) on the bulk structure. As is shown in the next section, the same two parameters are also responsible for the different types of Chl *a* aggregate organization.

Spectral characteristics of Chl *a* solubility and aggregation

In order to find a correlation between the solvent parameters and the type of Chl aggregates we compared the spectral characteristics at two important values of mole fractions of water established from Fig. 1. In all mixtures, at the onset and completion of transition, all Chl molecules are in monomeric and fully aggregated states, respectively. At these points, the interactions with and/or between solvent and water molecules are expected to be responsible for differences in the state of Chl *a.*

Chl a *in pure solvents and at the onset of transition.* The comparison of spectra 1 and 2 in Fig. 2 for all samples shows that the increase in water content up to the onset values (see Table 4 for the respective values) has the most profound effect on the Soret band intensity (ϵ_s). It is well established that the hydrogen bonding of solvent molecules at the carbonyl oxygen of the isocyclic ring changes the absorption spectra markedly (23). Renge and Avarmaa (23) have found an inverse linear correlation between ϵ_s and the solvent pa-
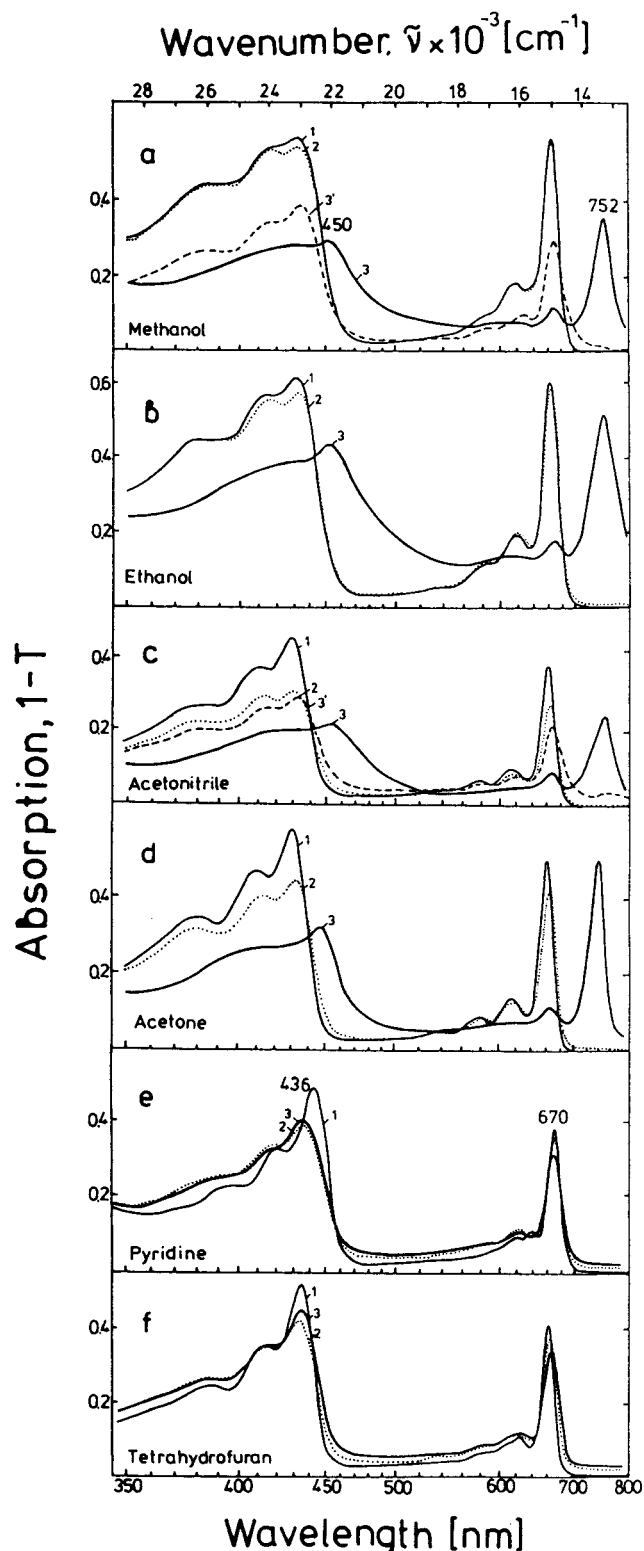

Figure 2. Absorption spectra of Chl *a* (1 − T, where T is the transmission) in the pure solvents (spectra 1 (——)) and in their mixtures with water at the onset (spectra 2 (····)) and at the completion of the monomer → aggregate transition when equilibrium was reached (spectra 3 (——)). Spectra 3′ (- - - -) in a and c are the spectra recorded just after the water admixing. The spectral transformations to the respective spectra 3 took 10–15 h and 8–10 h, respectively. See Table 4 for the respective values of mole fractions of water. The Chl concentration was 2.7–5.7 × 10^{-6} *M*.

Table 4. Spectral characteristics of Chl *a* in solvent–water mixtures at different mole fractions of water *f* when the equilibrium was reached

Solvent	Mole fraction water, f	Concentration of water (vol%)	Soret band position (±0.4 nm)	Q_y band position (±0.5 nm)	Q_y band FWHM (±16 cm^{-1}) (±0.5 nm)	Ratio Soret/Soret′ $\epsilon_s/\epsilon_{s'}$ (±0.01)	Ratio Soret/Q_y ϵ_s/ϵ_r (±0.01)	Fluorescence band position (±0.3 nm)	Main fluorescence band FWHM (±0.5)	Fluorescence lifetime τ_f* (±0.2 ns)
MeOH	0	0	431.5	665.7	520 (22.8)	1.05	1.0	674	24	6.0
Onset	0.43	25	431.5	666.7	528 (23.3)	1.02	0.97	675.5	25	5.8
End (spectrum 3)	0.69	50	450	752	664 (35.9)	1.12	0.77			0.1
EtOH	0	0	431	665	488 (21.5)	1.15	1.04	674	23	6.15
Onset	0.64	35	433	666	520 (23.2)	1.05	0.99	675	24	5.85
End	0.83	60	454	753	856 (49.0)	1.20	0.74			0.25
ACN	0	0	430.5	661.7	464 (20.2)	1.29	1.24	669	20.5	6.10
Onset	0.75	50	431.5	665.3	528 (23.3)	1.04	1.07	672	24	6.00
End (spectrum 3)	0.87	70	455	753	800 (45.4)	1.14	0.89			0.25
ACE	0	0	429.6	661.7	424 (18.1)	1.36	1.23	669	20	6.15
Onset	0.77	45	432	664.9	480 (21.1)	1.09	1.05	672	24	5.95
End	0.87	60	447.2	742	464 (26.3)	1.20	0.54			1.6; 0.1†
PYR	0	0	443.3	670.8	428 (19.1)	1.68	1.37	676.5	20	6.80
Onset	0.82	50	436.7	670.2	520 (23.3)	1.19	1.13	675.5	24	5.95
End	0.95	80	436	670	608 (28.0)	1.35	1.39			0.1
THF	0	0	435.6	664.5	408 (18.0)	1.66	1.34	669	19	6.85
Onset	0.82	50	434.7	666	464 (20.6)	1.28	1.17	673	21.5	6.50
End	0.95	80	436	666.7	584 (26.0)	1.41	1.43			0.1

*Measured after cut-off filter 660 nm.
†Measured after cut-off filter 710 nm.

Table 5. Coordination number of the Mg atom and hydrogen bonding of Chl *a* short wavelength-absorbing forms

Solvent/water mixtures	$\epsilon_s/\epsilon_{s'}$	Soret band FWHM	$\lambda(\frac{1}{4}\text{Soret})$ (nm)	$\dfrac{\epsilon(S_2 \leftarrow S_0, L_2)}{\epsilon(S_{21} \leftarrow S_0, L_1)}$	Predominant type of solvate
MeOH	1.05	86	452	1.64	L_2H
Onset	1.02	88	453	1.61	L_2H
End (spectrum 3′)	1.16	89	456	1.38	L_1H
EtOH	1.15	77	449	1.36	L_1H
Onset	1.05	86	451	1.33	L_1H
End*	1.12	93	457	1.37	L_1H
ACN	1.29	64	444	1.00	L_1
Onset	1.04	85	450	1.12	L_1H
End (spectrum 3′)	1.11	84	453	1.17	L_1H
ACE	1.36	44	442	1.00	L_1
Onset	1.09	78	447	1.14	L_1H
PYR	1.68	38	455	2.23	L_2
Onset	1.19	84	457	1.61	L_2 and L_1H (weak)
End (spectrum 3)	1.35	72	455	1.68	L_2
THF	1.66	39	450	1.90	L_2
Onset	1.28	70	450	1.90	L_2
End (spectrum 3)	1.41	47	451	1.78	L_2

*Observed at the instant of 50% water admixing and concentration of Chl *a* 3×10^{-5} *M*.

rameter E, while $\epsilon_{s'}$ changes little in different solvents. Based on this, the authors concluded that the ratio $\epsilon_s/\epsilon_{s'}$ can be considered as a measure of the strength of hydrogen-bonding interactions of Chl *a* with electrophilic solvent molecules. Because the added electrophilic molecules are the water molecules, the values of $\epsilon_s/\epsilon_{s'}$ (Table 4) reflect the degree of Chl *a* hydration. This ratio is very similar in MeOH, EtOH, ACN and ACE (1.02–1.09), while in PYR and THF it is considerably higher (1.19–1.28). The degree of hydration of monomeric Chl *a* in different solvent–water mixtures decreases in the order MeOH > EtOH = ACN > ACE > PYR > THF.

The decrease of $\epsilon_s/\epsilon_{s'}$ accompanied with the concomitant increase of Soret band FWHM (full width at half maximum) is established by Renge and Avarmaa (23) as a marker for the existence of hydrogen bonding mainly to the Chl *a* keto carbonyl group (see the original paper for the respective spectral values and solvent parameters). Table 5 presents the assignment of the hydrogen bonding based on these spectral features.

The assignment of a coordination number 5 or 6 to the Mg atom, *i.e.* L_1 or L_2 types of specific solvates of Chl *a*, was based on the other two semiquantitative indices of the absorption spectra introduced by Renge and Bitova (24). The relative content of L_2 and L_1 solvates can be determined from the ratio $\epsilon(S_2 \leftarrow S_0, L_2)/\epsilon(S_{21} \leftarrow S_0, L_1)$. The value of $\epsilon(S_2 \leftarrow S_0, L_2)$ is taken at the wavelength of the minimum between the $S_1 \leftarrow S_0$ (Q_y) and $S_{11} \leftarrow S_0$ bands (usually at ~610 nm); the value of $\epsilon(S_{21} \leftarrow S_0, L_1)$ is taken at the wavelength where there is a maximum of the $S_{21} \leftarrow S_0$ band of the Chl $a \cdot L_1$ complex (usually at ~580 nm). It is important to note that recently Umetsu *et al.* (39) have confirmed the sensitivity of these spectral regions to the coordination state of Chl *a*. An additional indication for the coexistence of L_2 and L_1 solvates is the wavelength (in red direction) at which the Soret band intensity is a quarter of the maximum ($\lambda[1/4$

Soret]). Table 5 presents the coordination number of Mg as determined with these indices. It is important to note that in pure solvents the same assignment of the coordination number of Mg and the hydrogen bonding of Chl *a* is derived when the resonance Raman (RR) markers are used (28,29). In this sense, the assignment of hydrogen-bonding and co-ordination interactions is well founded by the RR data.

In all mixtures at the onset of transition, with exception of THF (Table 4), the changes in absorption characteristics are accompanied with a 20% increase in the fluorescence band FWHM and the reduction of fluorescence lifetime τ_f to the values close to those in MeOH and EtOH. It was found that the existence of hydrogen bonding with solvent remarkably (30–40%) increases the FWHM of the main fluorescence band of Chl *b* at 5 K (40). The effect is the same for Chl *a* at room temperature (35). A 20–25% increase in FWHM was established by comparing the fluorescence spectra of Chl *a* in polar solvents with and without hydrogen-bond donating ability. Such differences cannot be explained solely by the effect of the dielectric constant. The same is seen with the comparison of fluorescence halfwidth in pure solvents (Table 4). The fluorescence lifetime is also solvent dependent (41), being lowest in alcohols and highest in aprotic polar solvents. In the case of nondegassed polar solvents, practically no difference exists between L_1 and $L_{1(2)}H$ solvates. Thus, these fluorescence parameters confirm the assignments presented in Table 5.

To sum up, at the onset of the transition, when the Chl is still in monomeric form, PYR and THF behave differently compared to the other four solvents in mixtures with water, not only by the lower degree of hydration, expressed by the higher values of $\epsilon_s/\epsilon_{s'}$, but also in their ability to stabilize the predominantly six-coordinated state of the Mg atom and by the absence of a strong hydrogen-bonded water molecule. This finding can be explained by the higher values of parameters P and B for PYR and THF. It is important to note that

the hydration of Chl *a* decreases in the same order just as the stabilization of hexacoordinated Mg increases in different solvent–water mixtures. Based on this, it can be concluded that maintaining Chl *a* in monomeric state is a balance between the hydration and preferential solvation by strongly nucleophilic solvents.

Chl a *aggregates in different mixtures before and when equilibrium was reached.* The spectral transformations in different solvents took different times after the addition of water. In EtOH, ACE, PYR and THF, the aggregates presented as spectra 3 in Fig. 2 were formed just after the water admixing. No additional spectral transformations were observed during prolonged monitoring (2 days). In MeOH and ACN after water admixing, the short-wavelength-absorbing aggregate appears (spectra 3′, Fig. 2) with characteristic red band tailing toward the longer wavelength region and the appearance of a small peak in that region. Its direct conversion to those presented with spectra 3 in Fig. 2 took 10–15 and 8–10 h, respectively. No additional transformations of spectra 3 were observed after prolonged standing (2 days). The state of aggregation in MeOH and EtOH was examined during a 1 week period. No changes in the shape of the spectra or in the absorption maxima were detected.

Comparison of the spectra at the completion of transition (spectra 3 in Fig. 2, Table 4) demonstrates the profound difference in the types of aggregates formed in MeOH–, EtOH–, ACN–, and ACE–water mixtures, on one side, and in PYR and THF, on the other side. Thus, the solvents can be divided into two groups based on their disparate effect on the type of Chl aggregate formation. The first group (MeOH, EtOH, ACE, ACN) in mixture with water gives rise to a strongly red-shifted Chl aggregate with Soret λ_{max} at 445–455 nm and Q_y λ_{max} at 742–753 nm (C750). The shape of the spectra in MeOH–, EtOH–, ACN–, and ACE–water mixtures (Fig. 2, spectra 3 and Table 4) is very similar. This spectral form is usually ascribed to the polymeric species of dihydrated Chl *a* (Chl $a \cdot 2H_2O)_n$ (8). The single Chl *a* molecule is hydrogen bonded to a water molecule and the second water molecule is the fifth ligand to the Mg of Chl *a*. Recently, Oba *et al.* (42) confirmed this assignment for the polar solvent–water mixture (aqueous 2-propanol) by using RR spectroscopy. Thus, the main conclusion from this comparison is that in the group I solvents, the water molecules succeed to replace the initial solvent molecules from the first solvation shell of Chl *a* giving rise to the polymeric aggregates of the type (Chl $a \cdot 2H_2O)_n$, while in group II (PYR and THF) water is not able to do this. Alfano *et al.* (43) have shown that the fluorescence lifetime of such aggregates can be used for estimation of their aggregation number. It is equal to the τ_f of the monomer divided by the τ_f of the aggregate. The time and intensity resolution of our apparatus for fluorescence lifetime measurements was insufficient for precise measurements on practically nonfluorescent probes. Nevertheless, the lifetimes presented in Table 4 can be used for rough estimation of the aggregate number. For ACE–water mixtures, the average fluorescence lifetime of the whole emission spectrum (using a 660 nm cut-off filter) was 1.6 ns, while in the long wavelength part of the spectrum (using a 710 nm cut-off filter) it was about 0.1 ns. This value yields an aggregate size of n > 60 molecules. For MeOH, EtOH and ACN, the signal was so small that it did not allow

us to measure in the long wavelength part of the emission spectrum. The lifetimes registered for the whole emission spectrum (using a 660 nm cut-off filter) for these mixtures (Table 4) suggest a larger size of aggregates (n > 100) compared with those in the ACE–water mixtures. These lifetime differences could be used to explain the difference in the absorption maximum, 742 nm for ACE and 752 nm for the other three solvents, with the different aggregation number. Note that the same difference in absorption spectra exists between ethyl- and methyl-chlorophyllide *a* microcrystals (44); nevertheless, both chlorophyllides occur as crystalline dihydrates.

In contrast, the spectra of Chl *a* with the group II solvent–water mixtures (Fig. 2, spectra 3e, 3f) and those formed at the initial stage of the aggregation with the group I solvents (Fig. 2, spectra 3′) as a whole differ slightly from the monomeric ones. The main differences in comparing the monomers in pure solvents are an increase in the ratio Soret/Q_y, with a concomitant decrease of the intensity of the Q_y band, an increase of light scattering and, of course, absence of fluorescence and extremely short fluorescence lifetimes. Compared with the form at the onset of the transition, the $\epsilon_s/\epsilon_{s'}$ ratio increases (clear indication for the decreased hydration of Chl), the Soret band halfwidth decreases and Q_y intensity decreases (ϵ_s/ϵ_r ratio increases, Tables 4 and 5). The spectra 3′ and spectra 3 of PYR and THF (Fig. 2) are identical to those of the typical colloidal aggregate of Chl *a* observed in various polar solvent–water mixtures (9,10,13,16,45). The exact location of the red absorption band in the 670–675 nm region and the ratio $\epsilon_s/\epsilon_{s'}$ depends on the conditions of mixing and the concentration of Chl. This dependence is also seen in the results for EtOH–water done at higher concentrations of Chl *a* and at different mixing conditions (Table 6). The fluorescence lifetimes of the transient colloidal aggregate C670 and of the C750 aggregate in MeOH and ACN are equal.

Based on the monomer-like absorption spectra of the C670 aggregate, it was possible to determine the coordination number of the Mg and the hydrogen bonding in the same way as described for monomeric Chl *a*. Table 5 presents these data and allows a comparison between the different observed absorption forms, both stable and transient. Thus, in contrast to the stable C750 aggregates and its precursor C670, this form in PYR and THF is built from predominantly six-coordinated Chl *a* by two solvent (not water) molecules, and H-bonding interactions do not play a decisive role in its stability. The absorption spectra of the transient aggregate C670 (spectra 3′, Fig. 2) is identical to that in aqueous dimethylsulfoxide (DMSO) (16). Koyama *et al.* (29) determined that Chl *a* in aqueous DMSO is five-coordinated and hydrogen bonded by using RR spectroscopy. In this sense, the assignment made here for the transient colloidal C670 aggregate is substantiated by RR data.

Comparison between the colloidal aggregates C670. The C670 aggregate in PYR and THF–water, (Chl $a \cdot L_2)_n$, and the transient C670 aggregate in MeOH and ACN-water, (Chl $a \cdot L_1 \cdot H_2O)_n$, also differ in their spectral parameter ϵ_s/ϵ_r and in the width of the red band (*cf.* Fig. 2, spectra 3 and 3′). Table 6 presents these data as well as a comparison with other systems. In both aggregates the absorption maximum is located at 670 nm, an indication that the π-electrons of

Table 6. Comparison of absorption characteristics of Chl a aggregates in aqueous media and in Chl a-enriched chloroplast fractions

System	Water content (vol/vol %) and Chl a concentration	λ Q$_Y$ (nm)	λ Soret (nm)	ϵ_s/ϵ_r	$\epsilon_s/\epsilon_{s'}$	$\epsilon_{s'}/\epsilon_r$	Q$_Y$ FWHM	Reference
Chl a monolayer at the water–Ar interface prepared by spreading an n-hexane solution of 10^{-5} M Chl a and 10^{-2} M EtOH on water, 22°C	Area per molecule at different pressure:							(46)
	125 Å^2 (4–5 dynes/cm)		437	1.21	1.18	1.02	34	
	98 Å^2 (22 dynes/cm)		438	1.31	1.24	1.04	34	
	37 Å^2 (27 dynes/cm), film collapsed		438	1.57	1.21	1.30	44	
Aqueous MeOH	60% water, Chl a = 5.7 × 10^{-6} M	669.5	435	1.32	1.16	1.14	32.6	This work
Aqueous EtOH	50% water, Chl a = 3 × 10^{-5} M	674	436	1.44	1.12	1.28	34.8	This work
Aqueous EtOH*	50% water, Chl a = 3 × 10^{-5} M	673	437	1.44	1.13	1.28	38.4	This work
Aqueous EtOH	70% water, Chl a = 3 × 10^{-5} M	673	436	1.43	1.06	1.35	36.5	This work
Aqueous ACN	70% water, Chl a = 2.9 × 10^{-6} M	669.5	434	1.46	1.11	1.32	32.2	This work
Aqueous PYR	80% water, Chl a = 2.7 × 10^{-6} M	670	436	1.39	1.35	1.03	28	This work
Aqueous THF	80% water, Chl a = 2.8 × 10^{-6} M	667	436	1.43	1.41	1.01	26	This work
chlorina f-2 mutant, chloroplasts in low salt buffer	Chl b-less mutant	680	437	1.52	1.09	1.49	30	(51)
chlorina f-2 mutant, thylakoid membranes	Chl b-less mutant	677	436	1.43	1.11	1.29	29.4	(52)
Photosystem I preparation, PS I(HA)-40 in buffer	Chl/P700 = 40, loss of Chl b	672	435	1.39	1.14	1.22	29	(53)
Photosystem I core complex, CCI	Chl a/Chl b (13.6/1), enriched in Chl a	676	438	1.38	1.15	1.20	29.4	(54)

*Chlorophyll a was dissolved in 0.05 mL EtOH, by first adding 0.35 mL H$_2$O and then adding 0.3 mL EtOH.

the adjacent molecules have no overlap. But as these aggregates differ in the number of the Mg axial ligands and the six-coordination can suppress the closeness of the macrocycles compared to the five-coordinated Mg, it is intuitively obvious that they can differ in their molecular packing density in the region of the chlorin macrocycles. In order to test this assumption, we compared the absorption parameters of Chl a monolayers at different pressures (46) that are also included in Table 6. It is clearly evident from the values of the absorption parameters corresponding to the area per molecule of 98 Å^2 and 37 Å^2 that the increase in the spectral parameter $\epsilon_{s'}/\epsilon_r$ and the width of the red band reflect the increased packing density. Thus, it can be concluded that aggregates of the type (Chl $a \cdot L_2$)$_n$ have a higher area per Chl molecule exposed to the water subphase compared with the aggregates of the type (Chl $a \cdot L_1 \cdot H_2O$)$_n$. On the other hand, it is known that the C750 form, (Chl $a \cdot 2H_2O$)$_n$, which is peculiar with its regular stacking of the Chl macrocycles and the shortest distance between them, has the smallest area per Chl molecule of 17 Å^2 (47).

If we compare the solvation parameters of PYR and THF with those of the other four solvents and water (Table 1), it is clear that they differ with respect to their nucleophilicity (B) and polarizability (P) parameters. Thus, it can be concluded that these parameters are important for the disparate effect the two groups of solvents have on the solubility and aggregation of Chl a in aqueous media.

How the environment modulates the type of Chl organization

The nonspecific polarizability parameter (P) is a function of the index of refraction of the medium, P = $(n^2 - 1)/(n^2 + 2)$, and reflects dipole-induced dipole interactions, according to classical dielectric theory (32). The larger the polarizability of a solvent, the greater its ability to bind to polarizable and weakly hydrophobic sites. For the case of Chl a, Seely and Jensen (26) have shown that aromatic molecules such as PYR and THF produce the greatest solvation effects on Chl that may result from some π complexation with the porphyrin ring. On the other hand, there is a well-established correlation between the polarizability of various low-molecular weight substances and their water structure-breaking activity (38,48). Obviously, both properties of highly polarizable solvents (PYR and THF)—a propensity for enhanced solvation of Chl a and the disruption of water structure—would be complimented in retaining the Chl in a monomeric state at higher water concentrations, when compared to solvents of group I, as well as preventing higher aggregation utilizing water molecules.

The nucleophilicity parameter (B) measures the Lewis basicity (nucleophilic solvating power, electron pair donating ability) of the solvent. It is similar to the well-known donor number parameter (21), and similarly, it is proportional to the strength of electron donor–acceptor interactions. As the Mg^{2+} of Chl a is the strongest electron-accepting center, the value of B is proportional to the strength of solvent–Mg coordination interaction. Thus, the higher polarizability and coordination abilities of PYR and THF, exerted *via* the preferential solvation and strong coordination interaction, maintain the hexacoordinated state of Mg and in this way prevent

Table 7. Uneven solvent distribution at the Chl a–water interface and in the bulk system for Chl a aggregates formed in the two groups of solvent–water mixtures

Solvent	Type of aggregate	Solvent/water mole ratio at the interface	Mole fractions of water in bulk	Solvent/water mole ratio in bulk system	Solvent distribution at the interface compared to the bulk
MeOH	C750 (Chl·2H$_2$O)$_{n>>2}$	0:2	0.69	1:2.3	Depletion
EtOH	C750 (Chl·2H$_2$O)$_{n>>2}$	0:2	0.83	1:4.88	Depletion
ACN	C750 (Chl·2H$_2$O)$_{n>>2}$	0:2	0.87	1:6.7	Depletion
ACE	C750 (Chl·2H$_2$O)$_{n>>2}$	0:2	0.87	1:6.7	Depletion
PYR	C670 (Chl·2PYR)$_{n>>2}$	2:0	0.95	1:19	Enrichment
THF	C670 (Chl·2THF)$_{n>>2}$	2:0	0.95	1:19	Enrichment

the higher hydration of monomeric Chl a at higher water content. The strong solvation of the Chl macrocycles by these monofunctional solvents does not allow strong macrocycle–macrocycle interactions mediated by water and the formation of higher aggregates C750 by using the water molecules. It is clear that the looseness of the molecular packing at the macrocycle region requires the involvement of phytol–phytol interactions for the relative stability of these aggregates in aqueous media.

Mechanism of Chl a dissolution and aggregation in aqueous media

Three main findings of this work: (1) the correlation between the structure of the medium and the aggregation of Chl a; (2) the graded response of the solvents with respect to the water content at the onset and the midpoint of Chl a monomer $\rightarrow$ aggregate transformation; (3) the differentiation of the solvents into two groups, based on the disparate effects that they exert on the Chl a aggregate organization, are a consistent advantage that permits the elucidation of the mechanism for Chl dissolution and aggregation in various aqueous media. The established ordering of solvents—MeOH < EtOH < ACN < ACE < PYR < THF—yields a typical lyotropic (Hofmeister) series (49). Much smaller amounts of THF and PYR are needed to disrupt medium structure (*i.e.* to keep the Chl monomer from associating with others) compared to the solvents on the left side of the order (MeOH, EtOH). The ability of many substances of low-molecular weight (salts, solvents, amino acids, *etc.*) to exhibit lyotropic effects on the solubility, stability and functional activity of biological macromolecules and biomolecular assemblies is well known (48,49). A large number of experimental studies show that the properties of the interface between aqueous and nonaqueous phases can be markedly affected *via* indirect interactions with added substances (49). These substances stabilize or destabilize the structure of bulk water (liquid) and thus influence the properties of interfacial water (the Hofmeister effect). The particular solvents in such series exert disparate effects on the behavior of biological macromolecules or biomolecular assemblies, depending on their position in the Hofmeister series, *i.e.* depending on their effect on bulk structure (48–50). The solvents on the left side of the Hofmeister series are termed kosmotropes (structure makers) and usually stabilize native protein conformation. In contrast, those on the right side of the series, termed chaotropes (structure breakers), destabilize native protein conformation. The tendency of Hofmeister solutes to

distribute unevenly between bulk system and interfaces is a well-known experimental fact (48,49). It is also generally recognized that kosmotropes favor the stability of conformations with reduced surface area, while chaotropes favor those with increased surface area. For the case of modulation of lipid-phase behavior by kosmotropes and chaotropes these experimental observations have recently been theoretically substantiated (50). The derived general thermodynamic equation provides a clear description in physical quantities of the disparate effects of the different substances on the lipid-phase behavior. According to that equation, kosmotropes and chaotropes have opposite effects on the lipid-phase behavior due to their uneven distribution between interfacial (bound) and bulk (free) water. Kosmotropes tend to be excluded from the interface, while chaotropes tend to accumulate at the interface. Kosmotropes favor the L$_\beta$ (gel) and the inverted hexagonal H$_{II}$ phases at the expense of the L$_\alpha$ (liquid crystalline) phase, as the former phases have reduced area per lipid molecule exposed to water. To the contrary, chaotropes tend to expand the lipid interface area and favor the L$_\alpha$ phase, as that phase has the largest area per lipid molecule.

It is evident from Table 7 that just as displayed in lipid-phase behavior, the two groups of solvents exert their disparate effects on Chl aggregate organization. The solvents from group I (MeOH, EtOH, ACE and ACN) act as kosmotropic substances. They stabilize the structure of bulk liquid (their position in the series) and tend to be excluded from the interfacial Chl–water regions (Table 7). In turn, this brings about a tendency to reduce the energetically unfavorable area of Chl–water contact. The surface area per Chl molecule is strongly reduced by the formation of the two-water hydrogen-bonding network that keeps the Chl macrocyles close to each other. These solvents favor the C750 aggregates at the expense of C670 as the former aggregate has the smallest surface area per Chl molecule at the interface between aqueous and nonaqueous phases. By the same argument, the solvents from group II (PYR and THF) act as chaotropes. They tend to disrupt the bulk structure (their position in the series), accumulate at the Chl interface and directly interact with Chl electrophilic interfacial group Mg^{2+} (Table 7). They support the C670 aggregate, as it has the largest area per Chl molecule exposed at the interface. Thus, based on these data concerning the disparate effect of solvents on Chl aggregates, we have shown that the mechanism for Chl self-assembly in aqueous media can be considered a manifestation of the Hofmeister effect, as displayed

in lipid-phase behavior (50). It relates on the solvent ability to modify the bulk structure and to distribute unevenly between the Chl–water interface and bulk liquid.

The proposed mechanism for modulation of Chl aggregates by kosmotropic and chaotropic cosolvents can explain the formation of special Chl aggregates absorbing in the 685–695 nm region that are formed only in certain polar solvent–water mixtures (9,16,17). A characteristic feature of these aggregates is that water does not participate as a ligand or in hydrogen bonding to the Chl molecule. Their stabilization can be explained by the chaotropic manner of action of either a bifunctional solvent such as dioxane or dimers of DMSO and THF, just as the chaotropes are able to induce and stabilize missing phases in the phase sequence of certain lipid–water systems (50). The proposed mechanism can also explain the observed suppressing effect of urea and imidazole on the formation of C690 aggregates in formamide–water systems (11), due to their strong chaotropic nature. This mechanism also explains the established inverse correlation (5) between the refractive index and the optimal concentration of the organic solvents effective in producing the 740 nm-absorbing Chl aggregates in chloroplast fragments.

How to correlate the present results on Chl aggregation in aqueous media with the Chl–Chl interactions observed in photosynthetic complexes

The main problem of many model studies is how to relate the observed results on Chl aggregation to the spectra–structure–function relationship with native systems. Usually, the stable dimers formed in particular aqueous solvents are suitable models for the reaction centers Chl *a*. It must be noted that the C750 aggregates and C670 in PYR and THF–water mixtures are not physiologically important species. They are only observed during the treatment of chloroplast fragments (5) or chlorosomes (3). As is evident from the comparison of absorption characteristics of Chl *a*-enriched preparations and Chl *b*-less mutants with those of the C670 aggregates studied here (Table 6), only the precursor of the C750 aggregates, *i.e.* the transient C670 aggregate of the type (Chl $a \cdot L_1 \cdot H_2O)_n$ can have a certain physiological importance. Its absorption characteristics ϵ_s/ϵ_r, $\epsilon_s/\epsilon_{s'}$, and $\epsilon_{s'}/\epsilon_r$, FWHM, the very low fluorescence quantum yield and fluorescence lifetime are very similar if not identical to those of the Chl *a in vivo* (*cf.* Table 6 and Holzwarth (55) for the fluorescence lifetimes of antenna Chl complexes). To the best of our knowledge, the close similarity in the absorption characteristics of ϵ_s/ϵ_r, $\epsilon_s/\epsilon_{s'}$, and $\epsilon_{s'}/\epsilon_r$ between the Chl *a* aggregates in aqueous media and Chl *a* in native systems is reported for the first time. In 1965 Clayton (56) suggested that the amorphous monolayers and colloidal Chl might be good models for Chl *a* aggregates *in vivo,* based on the close similarity in the positions of absorption maxima. In addition to his hypothesis, we point out that only a metastable Chl organization, *i.e.* Chl aggregate organization at the boundary of its stability, could explain the finding that antenna Chl *a* has a structural role in stabilizing the functional conformation of P700–chlorophyll–protein complexes (57), as well as the appearance of 740 nm Chl forms during the treatment of chloroplast fragments with kosmotropic solvents (5).

In the present work, the main focus was on finding a correlation between the structure and properties of the medium and the process of Chl aggregation and, in this way, shed light on the possible mechanism for Chl aggregation in aqueous media. In this regard, another aspect of the relevance to *in vivo* systems is reported here. In the present work, it is found that Chl association and stabilization of different aggregated forms are governed by the same mechanism as those that modulate the organization and stability of the other two components of photosynthetic membranes: lipids and proteins. In this sense, the results presented here are mainly of importance to indirect studies of pigment organization *in vivo*. The strength of Chl–Chl (Bchl–Bchl) interactions in the photosynthetic complexes can be modulated subtly by varying the nature of additives to the system. These interactions can be influenced by pH, salt concentration, buffer and different stress conditions (high and low temperature, dehydration, *etc.*). Thus, the connection between these model systems and the native ones is the common mechanism modulating their stability.

The power of this common mechanism can be further exemplified by the explanation of the experimental fact that the glycolipid monolayer is not destroyed during the 1-hexanol treatment of the native chlorosomes (58), while the Bchl *c, d* aggregates absorbing at 740–750 nm are converted to 670 nm-absorbing aggregates (4). It is known that at low concentrations, all solvents behave as water structure breakers: they interact with water and disrupt the normal type of long-range order (38). Thus, the conversion of 740–750 nm-absorbing Bchl *c, d* species can be explained by the enrichment of Bchl interfacial regions with 1-hexanol that stabilizes the aggregates absorbing at 670 nm, very similarly to those considered here. On the other hand, the inversion point in the Hofmeister series for glycolipid dispersions in water is positioned at the chaotropic end of the Hofmeister series (50). The sign inversion point in these series depends on the effect of the particular biomolecule on the structure of water (50,59). Compared with other lipid classes and Chl *a,* the effect of chaotropes on the stability of glycolipid phases is the smallest one. This explains why the addition of 1-hexanol does not affect the glycolipid monolayer structure of chlorosomes.

REFERENCES

1. Olson, J. M. (1998) Chlorophyll organization and function in green photosynthetic bacteria. *Photochem. Photobiol.* **67**, 61–75.
2. Paulsen, H. (1995) Chlorophyll *a/b*-binding proteins. *Photochem. Photobiol.* **62**, 367–382.
3. Brune, D. C., T. Nozawa and R. E. Blankenship (1987) Antenna organization in green photosynthetic bacteria. 1. Oligomeric bacteriochlorophyll *c* as a model for the 740 nm absorbing bac-

teriochlorophyll *c* in *Chloroflexus aurantiacus* chlorosomes. *Biochemistry* **26**, 8644–8652.

4. Zhu, Y., S. Lin, B. L. Ramakrishna, P. I. van Noort and R. E. Blankenship (1996) Self quenching of chlorosome chlorophylls in water and hexanol-saturated water. *Photosynth. Res.* **47**, 207–218.

5. Lippincott, J. A., J. Aghion, E. Porcile and W. F. Bertsch (1962) The preparation and characterization of chloroplast fragments having an absorbancy maximum at 7400 Å. *Arch. Biochim. Biophys.* **98,** 17–27

6. Dijkmans, H. and J. Aghion (1974) Conditions de formation d'agrégats de chlorophylle *a* dans des solvants polaires aqueux: polarité du milieu. *Plant & Cell Physiol.* **15**, 739–745.

7. Scherz, A., V. Rosenbach-Belkin and J. R. E. Fisher (1991) Chlorophyll aggregation in aqueous solutions. In *Chlorophylls* (Edited by H. Scheer), pp. 237–268. CRC Press, Boca Raton, FL.

8. Katz, J. J., M. K. Bowman, T. J. Michalski and D. L. Worcester (1991) Chlorophyll aggregation: chlorophyll/water micelles as models for *in vivo* long-wavelength chlorophyll. In *Chlorophylls* (Edited by H. Scheer), pp. 211–235. CRC Press, Boca Raton, FL.

9. Love, B. B. (1962) Absorption spectra of chlorophyll *a* in aqueous carbitol solutions. *Biochim. Biophys. Acta* **64**, 318–323.

10. Love, B. B. and T. T. Bannister (1963) Studies of colloidal chlorophyll in aqueous dioxane. *Biophys. J.* **3**, 99–113.

11. Quilman, K. P. (1968) Aggregation of chlorophylls in aqueous-formamide solutions. *Arch. Biochim. Biophys.* **127**, 31–36.

12. Journeaux, R., A. Hochapfel and R. Viovy (1969) Existence et nature des formes agrégées de la chlorophylle *a* dans les solvants binaires. II—Étude des spectres de fluorescence. *J. Chim. Phys.* **66**, 1474–1478.

13. Hochapfel, A., R. Journeaux and R. Viovy (1969) Existence et nature des formes agrégées de la chlorophylle *a* dans les solvants binaires. I.—Étude des spectres d'absorption. *J. Chim. Phys.* **66**, 1467–1473.

14. Vladkova, R. and S. Taneva (1988) Spectral characteristics of chlorophyll *a* at different states of solvation. In *Electromagnetic Fields and Biomembranes* (Edited by M. Markov and M. Blank), pp. 267–271. Plenum Press, New York and London.

15. Agostiano, A., P. Cosma and M. Della Monica (1990) Spectroscopic and electrochemical characterization of chlorophyll *a* in different water + organic solvent mixtures. *Bioelectrochem. Bioenerg.* **23**, 311–324.

16. Uehara, K., M. Mimuro and M. Tanaka (1991) Spectroscopic studies of chlorophyll *a* aggregates formed by aqueous dimethyl sulfoxide. *Photochem. Photobiol.* **53**, 371–377.

17. Uehara, K., Y. Hioki and M. Mimuro (1993) The chlorophyll *a* aggregate absorbing near 685 nm is selectively formed in aqueous tetrahydrofuran. *Photochem. Photobiol.* **58**, 127–132.

18. Agostiano, A., M. Della Monica, G. Palazzo and M. Trotta (1993) Chlorophyll *a* autoaggregation in water rich region. *Biophys. Chem.* **47**, 193–202.

19. Balny, C., S. S. Brody and G. H. B. Hoa (1969) Absorption and fluorescence spectra of chlorophyll-*a* in polar solvents as a function of temperature. *Photochem. Photobiol.* **9**, 445–454.

20. Oba, T., M. Mimuro, Z.-Y. Wang, T. Nozawa, S. Yoshida and T. Watanabe (1997) Spectral characteristics and colloidal properties of chlorophyll *a'* in aqueous methanol. *J. Phys. Chem. B* **101**, 3261–3268.

21. Gutman, V. (1978) *The Donor–Acceptor Approach to Molecular Interactions.* Plenum Press, New York.

22. Reichardt, C. (1979) *Solvent Effects in Organic Chemistry.* Verlag Chemie, Weinheim.

23. Renge, I. and R. Avarmaa (1985) Specific solvation of chlorophyll *a*: solvent nucleophility, hydrogen bonding and steric effects on absorption spectra. *Photochem. Photobiol.* **42**, 253–260.

24. Renge, I. V. and Ye. V. Bitova (1987) Solvation of chlorophylls by solvents modelling the protein environs. *Biophysics* **32**, 403–408.

25. Callahan, P. M. and T. M. Cotton (1987) Assignment of bacteriochlorophyll *a* ligation state from absorption and resonance Raman spectra. *J. Am. Chem. Soc.* **109**, 7001–7007.

26. Seely, G. R. and R. G. Jensen (1965) Effect of solvent on the spectrum of chlorophyll. *Spectrochim. Acta* **21**, 1835–1845.

27. Dähne, S., W. Becker, M. Scholz, K. Teuchner, H. Lunch and H. Schneider (1980) Impuls Fluorometer auf Laserbasis. *Feingerätetechnik.* **29**, 463–466.

28. Fujiwara, M. and M. Tasumi (1986) Resonance Raman and infrared studies on axial coordination to chlorophylls *a* and *b* in vitro. *J. Phys. Chem.* **90**, 250–255.

29. Koyama, Y., Y. Umemoto, A. Akamatsu, K. Uehara and M. Tanaka (1986) Raman spectra of chlorophyll forms. *J. Mol. Struct.* **146**, 273–287.

30. Åkerlöf, G. (1932) Dielectric constants of some organic solvent–water mixtures at various temperatures. *J. Am. Chem. Soc.* **54**, 4125–4139.

31. Hasted, J. B. (1973) Dielectric properties. In *Water. A Comprehensive Treatise,* Vol. II, *Water in Crystalline Hydrates; Aqueous Solutions of Simple Nonelectrolytes* (Edited by F. Franks), Chapter 7, pp. 405–458. Plenum Press, New York.

32. Palm, V. A. (1977) *The Fundamentals of the Quantitative Theory of Organic Reactions.* Khimia Publishing House, Leningrad.

33. Reichardt, C. and K. Dimroth (1968) Lösungsmittel und empirische Parameter zur Charakterisierung ihrer Polarität. *Fortschr. Chem. Forsch.* **11**, 1–73.

34. Köhler, W., P. Frölich and R. Radeglia (1969) Korrelation der chemischen Verschiebung der Wasserprotonen im NMR-Spektrum von Aceton-, 1,4-Dioxan-, und Tetrahydrofuran-Wasser-Gemischen mit empirischen Parametern der Lösungsmittelpolarität. *Z. Phys. Chem.* **242**, 220–224.

35. Vladkova, R. (1990) Influence of local environment on the spectral characteristics of chlorophylls. Ph.D. Thesis, Institute of Biophysics, Bulgarian Academy of Sciences, Sofia.

36. Szabo, A. G. and D. M. Rayner (1980) Fluorescence decay of tryptophan conformers in aqueous solution. *J. Am. Chem. Soc.* **102**, 554–563.

37. Suppan, P. (1990) Solvatochromic shifts: the influence of the medium on the energy of electronic states. *J. Photochem. Photobiol. A Chem.* **50**, 293–330.

38. Franks, F. (ed.) (1973) *Water. A Comprehensive Treatise,* Vol. II: *Water in Crystalline Hydrates; Aqueous Solutions of Simple Nonelectrolytes.* Plenum Press, New York.

39. Umetsu, M., Z.-Y. Wang, M. Kobayashi and T. Nozawa (1999) Interaction of photosynthetic pigments with various organic solvents. Magnetic circular dichroism approach and application to chlorosomes. *Biochim. Biophys. Acta* **1410**, 19–31.

40. Vladkova, R. S., K. H. Mauring and I. V. Renge (1989) Specific solvation of chlorophyll *b*: a site-selection study at 5 K. *J. Photochem. Photobiol. B Biol.* **3**, 25–31.

41. Seely, G. R. and J. S. Connolly (1986) Fluorescence of photosynthetic pigments *in vitro*. In *Light Emission by Plants and Bacteria* (Edited by Govindjee), pp. 99–133. Academic Press, New York.

42. Oba, T., H. Furukawa, Z.-Y. Wang, T. Nozawa, M. Mimuro, H. Tamiaki and T. Watanabe (1998) Supramolecular structures of the chlorophyll *a'* aggregate and the origin of the diastereoselective separation of chlorophyll *a* and *a'*. *J. Phys. Chem. B* **102**, 7882–7889.

43. Alfano, A. J., F. E. Lytle, M. S. Shoewell and F. K. Fong (1985) Excited singlet-state lifetimes of hydrated chlorophyll aggregates. *J. Chem. Phys.* **82**, 758–764.

44. Kratky, C. and J. D. Dunitz (1977) Ordered aggregation states of chlorophyll *a* and some derivatives. *J. Mol. Biol.* **113**, 431–442.

45. Kadoshnikova, I. G. and B. A. Kiselev (1979) Colloidal solutions of chlorophyll. Electric charge of the particles. *Biofizika* **24**, 811–814.

46. Heithier, H., K. Ballschmiter and H. Möhwald (1983) Liquid-crystalline phase transition of monomolecular layers of chlorophyll *a*. *Photochem. Photobiol.* **37**, 201–205.

47. Ke, B. (1966) Some properties of chlorophyll monolayers and crystalline chlorophyll. In *The Chlorophylls* (Edited by L. P. Vernon and G. R. Seely), pp. 253–279. Academic Press, New York.

48. Cacace, M. G., E. M. Landau and J. J. Ramsden (1997) The

Hofmeister series: salt and solvent effects on interfacial phenomena. *Q. Rev. Biophys.* **30**, 241–277.

49. Collins, K. D. and M. W. Washabaugh (1985) The Hofmeister effect and the behaviour of water at interfaces. *Q. Rev. Biophys.* **18**, 323–422.
50. Koynova, R., J. Brankov and B. Tenchov (1997) Modulation of lipid phase behavior by kosmotropic and chaotropic solutes. Experiment and thermodynamic theory. *Eur. Biophys. J.* **25**, 261–274.
51. Searle, G. F. W., C. J. Tredwell, J. Barber and G. Porter (1979) Picosecond time-resolved fluorescence study of chlorophyll organization and excitation energy distribution in chloroplasts from wild-type barley and a mutant lacking chlorophyll *b*. *Biochim. Biophys. Acta* **545**, 496–507.
52. Garab, G., J. Kieleczawa, J. C. Sutherland, C. Busramante and G. Hind (1991) Organization of pigment–protein complexes into macrodomains in the thylakoid membranes of wild-type and chlorophyll *b*-less mutant of barley as revealed by circular dichroism. *Photochem. Photobiol.* **54**, 273–281.
53. Baba, K., S. Itoh, G. Hastings and S. Hoshina (1996) Photo-inhibition of Photosystem I electron transfer activity in isolated Photosystem I preparations with different chlorophyll contents. *Photosynth. Res.* **47**, 121–130.
54. Preiss, S., G. F. Peter, S. Anandan and J. P. Thornber (1993) The multiple pigment-proteins of the photosystem I antenna. *Photochem. Photobiol.* **57**, 152–157.
55. Holzwarth, A. R. (1991) Excited-state kinetics in chlorophyll systems and its relationship to the functional organization of the photosystems. In *Chlorophylls* (Edited by H. Scheer), pp. 1125–1151. CRC Press, Boca Raton, FL.
56. Clayton, R. K. (1965) *Molecular Physics of Photosynthesis,* Chapter 12, pp. 149–164. Blaisdell Publ. Co., New York.
57. Ikegami, I. and S. Katoh (1991) Antenna chlorophyll *a* has a structural role in stabilizing the functional conformation of P-700-chlorophyll–protein complexes. *Biochim. Biophys. Acta* **1059**, 275–280.
58. Zhu, Y., B. L. Ramakrishna, P. I. van Noort and R. E. Blankenship (1995) Microscopic and spectroscopic studies of untreated and hexanol-treated chlorosomes from *Chloroflexus aurantiacus. Biochim. Biophys. Acta* **1232**, 197–207.
59. Komsa-Penkova, R., R. Koynova, G. Kostov and B. G. Tenchov (1996) Thermal stability of calf skin collagen type I in salt solutions. *Biochim. Biophys. Acta* **1297**, 171–181.